Published in final edited form as:

Free Radic Biol Med. 2010 September 15; 49(6): 1119–1128. doi:10.1016/j.freeradbiomed.2010.06.030.

ICAM-1 cytoplasmic tail regulates endothelial glutathione synthesis through a NOX4/PI3-kinase-dependent pathway

Christopher B. Pattillo[a], **Sibile Pardue**[a], **Xinggui Shen**[a], **Kai Fang**[a], **Will Langston**[a], **David Jourd'heuil**[b], **Terrance J. Kavanagh**[c], **Rakesh P. Patel**[d], and **Christopher G. Kevil**[a,*]

[a]Department of Pathology, Louisiana State University Health Sciences Center at Shreveport, Shreveport, LA 71130, USA

[b]Center for Cardiovascular Sciences, Albany Medical College, Albany, NY 12208, USA

[c]Department of Environmental and Occupational Health Sciences, University of Washington, Seattle, WA 98195, USA

[d]Department of Pathology and Center for Free Radical Biology, University of Alabama at Birmingham, Birmingham, AL 35294, USA

Abstract

We previously reported that ICAM-1 expression modulates endothelial intracellular glutathione (GSH) metabolism through unknown mechanisms. Here we report that the cytoplasmic tail of ICAM-1 is critically involved in governing intracellular GSH production. Peptides containing the antennapedia cell-permeative sequence (AP) or an AP peptide linked to the transmembrane and cytosolic tail of ICAM-1 (AP-ICAM) were synthesized and used to measure alterations in redox status in cultured endothelial cells and determine their biological effect. Treatment with AP-ICAM significantly increased GSH concentrations and glutamate–cysteine ligase (GCL) activity over time. Measuring reactive oxygen species (ROS) production with DCF revealed a rapid increase in ROS generation after AP-ICAM treatment. Measurement of superoxide production with hydroethidium revealed biphasic production at 30 min and 6 h after treatment with AP-ICAM. Apocynin, DPI, catalase, or SOD attenuated AP-ICAM-dependent ROS production, GCL activity, and GSH production, implicating superoxide production and dismutation to peroxide. Consistent with these findings, NOX4 siRNA knockdown blocked AP-ICAM peptide increases in GSH or GCL activity, demonstrating the importance of NADPH oxidase. Last, inhibition of PI3-kinase activity with LY 294002 or wortmannin blocked AP-ICAM GSH induction and ROS production. These data reveal that the ICAM-1 cytoplasmic tail regulates production of endothelial GSH through a NOX4/PI3-kinase-dependent redox-sensitive pathway.

Keywords

Intercellular adhesion molecule-1; GSH; Superoxide; Endothelium; VEGF chemotaxis; Free radicals

*Corresponding author. Fax: +1 318 675 7662. ckevil@lsuhsc.edu (C.G. Kevil).

The role of oxidative stress as a critical pathophysiological mediator in cardiovascular disease (CVD) is widely appreciated [1]. Oxidant-dependent endothelial cell activation plays an important role in mediating the biological responses of angiogenesis and inflammation, which both contribute to CVD [2–4]. Conversely, intracellular antioxidant networks, such as glutathione, are decreased during CVD, highlighting the importance of redox regulation for cardiovascular homeostasis and normal endothelial cell function [5].

The tripeptide glutathione (GSH) is the most abundant intracellular antioxidant and is formed by the rate-limiting, heterodimeric enzyme glutamate cysteine ligase (GCL) [6]. GSH serves critical roles in regulating oxidative insult and reactive oxygen species (ROS)-induced signaling and is associated with antiproliferative and anti-inflammatory properties in CVD [7,8]. Few studies have identified endogenous antioxidant pathways that are specifically found in the cardiovascular system or their effects on endothelial cell responses (e.g., angiogenic activation) involved during cardiovascular pathophysiology.

An important source of ROS during CVD is NADPH oxidase, which serves important roles in governing endothelial cell responses during angiogenesis and inflammation [9]. Vascular endothelial growth factor (VEGF), a proangiogenic factor, is produced in response to increased ROS production, thereby priming endothelial cells to adopt a proangiogenic state [10–12]. VEGF binds to VEGFR2 on the surface of endothelial cells and activates several downstream signaling pathways leading to endothelial cell migration, proliferation, and angiogenesis [13]. Likewise, VEGF binding to its ligand VEGFR2 leads to NADPH oxidase activation and production of superoxide ($O_2^{\bullet -}$), which facilitates angiogenesis responses such as endothelial cell migration and proliferation [14–18].

Experiments have shown that inflammatory adhesion molecules (e.g., ICAM-1) modulate endothelial cell angiogenic activity through unknown mechanisms [19–21]. Work from our laboratory suggests that ICAM-1 expression can regulate endothelial cell angiogenic activity by controlling endothelial cell redox status through increasing intracellular GSH levels [22–24]. In our previous studies, we examined endothelial cells from ICAM-1 gene-targeted mutant mice, which are devoid of functional ICAM-1 expression but can express alternatively spliced isoforms of ICAM-1, resulting in truncated nonbinding membrane-spanning peptides containing an intact cytoplasmic tail [23,25]. Thus, we considered whether ICAM-1-dependent alterations in cellular redox status could be related to the presence of truncated ICAM-1 containing the cytoplasmic tail that can participate in various signaling responses [26]. The notion that the cytoplasmic tail of ICAM-1 endogenously regulates endothelial cell GSH metabolism suggests a novel redox regulatory mechanism and provides an exciting avenue to explore in activating endogenous antioxidant defense pathways as an innovative therapy for cardiovascular disease. Herein we present evidence that the ICAM-1 cytoplasmic tail is a potent regulator of endothelial cell redox status by increasing intracellular GSH levels and enhancing glutamate cysteine ligase enzyme activity, which strongly impacts endothelial cell angiogenic activity.

Experimental procedures

Materials

The murine microvascular endothelial cell line MS-1 was obtained from ATCC (Manassas, VA, USA) and cultured in DMEM (Mediatech, Herndon, VA, USA) supplemented with 5% fetal calf serum and an L-glutamine, penicillin–streptomycin solution (Sigma, St. Louis, MO, USA). The cell-permeative indicator 5-(and 6-)chloromethyl-2′,7′-dichlorodihydrofluorescein diacetate, acetyl ester (DCF) was used to measure ROS and was purchased from Molecular Probes (Carlsbad, CA, USA). Buthionine sulfoximine (BSO), diphenyleneiodonium (DPI), wortmannin, PEG–superoxide dismutase (SOD), and PEG–catalase were obtained from Sigma Chemical. LY 294002 was purchased from CalBiochem. The antennapedia (AP), AP-ICAM, TD1, TD2, and TD3 peptides were synthesized by PolyPeptide Laboratories (San Diego, CA, USA). GAPDH antibody was purchased from Cell Signaling (Danvers, MA, USA), and horseradish peroxidase (HRP)-conjugated anti-rabbit IgG was purchased from Sigma. Aprotinin, leupeptin, okadaic acid, phenylmethylsulfonyl fluoride, and phosphatase inhibitor cocktail were also purchased from Sigma.

Cell culture

Cells were routinely passaged and maintained in DMEM supplemented with 5% fetal calf serum and L-glutamine, penicillin–streptomycin solution. Cells were plated according to assay parameters outlined below to determine ROS concentration, GCL activity, and GSH and catalytic subunit of GCL (Gclc) levels.

Measurement of GSH levels and GCL activity

Confluent monolayers of cells were serum depleted (0.5% serum in medium) and treated with or without 150 μM BSO for 16 h. In a separate set of experiments, cells were pretreated with apocynin (100 μM), wortmannin (6 μM), or LY 294002 (20 μM) 30 min before treatment with various peptides to evaluate the role of ROS or PI3-kinase activity in modulating GSH levels/GCL activity. Measurement of both GSH and GCL activity was performed as reported by White et al. at various time points [27]. Briefly, cells were washed, trypsinized, pelleted, and lysed by sonication. So as not to be limiting for the synthesis of γ-glutamylcysteine (γ-GC), cysteine, glutamate, and ATP concentrations in the GCL reaction cocktail were above the K_m for mouse Gclc. GCL activity reactions were carried out at 37 °C for 45 min. Protein was then acid precipitated and supernatants were reacted with naphthalene dicarboxaldehyde and added to a 96-well plate, and fluorescence was measured using a Tecan Genios Plus plate reader. GSH and γ-GC concentrations are reported as nanomoles per milligram of protein or fold change over vehicle.

Measurement of reactive oxygen species formation

Cells were plated in 24-well dishes and allowed to reach confluence. The cells were then placed in a reduced-serum environment (0.5% serum) for 16 h and experiments were conducted using serum and phenol red-free medium buffered with Hepes. Cells were labeled with a 10 μM solution of DCF for 30 min (with unlabeled controls) and then washed three

times with PBS to remove excess DCF. In one set of experiments, DCF-labeled cells were pretreated with either 100 μM apocynin or 1 μM DPI for 15 min before treatment with the various peptides. In a separate set of experiments DCF-labeled cells were pretreated with either PEG–SOD (400 units/ml) or PEG–catalase (100 units/ml) for 30 min before the various peptide treatments. Medium alone or supplemented with AP peptide (25 μM) or AP-ICAM peptide (25 μM) was placed on the cells and measurements were taken with a Tecan Genios fluorescence plate reader in 10-min intervals for the first 30 min and then in 30-min intervals for 180 min.

Intracellular superoxide production was measured using the hydroethidine (HE) method as previously published by Zielonka et al. [28], which was quantified by HPLC. Briefly, cells were treated with vehicle, AP peptide, AP-ICAM peptide, or PBS for various times and then incubated with cell culture medium containing 10 μM HE for 30 min. Cells were then washed with PBS, pelleted, and lysed with a Triton X-100 solution. Proteins in the solution were precipitated using acidified methanol and the 2-OH-ethidium (2-OH-E) product was measured using fluorescence detection (ex 490 nm, em 567 nm) with a Shimadzu UFLC HPLC system. 2-OH-E superoxide production was normalized to total protein.

Protein carbonyl formation was measured using the commercial protein carbonyl ELISA kit from Cell Biolabs (San Diego, CA, USA) according to the manufacturer's instructions. Thirty micrograms of total protein was used per treatment condition per sample to measure protein carbonyl. Data are reported as nanomoles of protein carbonyl per milligram of total protein.

PI3-kinase activity assay

PI3-kinase activity was measured using an ELISA kit from Echelon Biosciences (Salt Lake City, UT, USA) with the following modifications. Cells were grown and treated with peptides as described above. Cells were lysed in 30 μl of ice-cold lysis buffer (20 mM Tris–HCl, pH 7.4, 137 mM NaCl, 1 mM $CaCl_2$, 1 mM $MgCl_2$, 1 mM sodium orthovanadate, and 1% NP-40). Thirty micrograms of total protein was mixed with an equal volume of 2× KBZ buffer and then brought up to a total volume of 55 μl with 1× KBZ buffer, which was commercially provided. The PI3 kinase activity was measured by addition of 8 μM PIP2 substrate to each sample and incubated for 2 h at 37 °C. The reaction was stopped and PIP3 antibody/EDTA (diluted according to the manufacturer's instructions) was added and incubated at room temperature for 1 h followed by secondary antibody labeling according to the manufacturer's instructions. The PIP3 ELISA was developed using the colorimetric reagent TMB and read on a plate reader at 450 nm.

Western blot analysis of Gclc expression

Western blots were performed as previously described [22]. Briefly 12 μg total protein was separated on a 10% SDS–polyacrylamide gel and transferred to a polyvinylidene difluoride membrane. Membranes were blocked for 8 h with 2% normal goat serum, 5% bovine serum albumin, 1% ova albumin, and 0.1% Tween. Membranes were washed and incubated overnight with anti-Gclc or -GAPDH antibodies at 1:5000 dilution. Membranes were washed three times with 0.1% normal goat serum and 0.1% Tween and then incubated with

HRP-linked goat anti-rabbit secondary antibody at 1:2000 dilution for 2 h. Membranes were then washed again and developed using ECL Western blot detection reagents.

Measurement of endothelial cell migration

Endothelial cell chemotaxis was performed as we have previously reported [22]. Falcon Fluoro-Block tissue culture inserts with 8-μm pores were plated with 33,000 endothelial cells each. Cells were treated with or without 150 μM BSO in 0.5% serum medium for 1 h before introduction of dimethyl sulfoxide (vehicle), AP peptide (25 μM), or AP-ICAM peptide (25 μM) and left for 16 h. Medium containing 0.5% serum and no phenol red was replaced and 10 μM Cell Tracker green was used to label the cells by incubating for 30 min at 37 °C. Inserts and wells were washed three times in PBS to remove excess Cell Tracker green. Cells were treated with or without mouse $VEGF_{164}$ (50 ng/ml); cells with no $VEGF_{164}$ received medium alone. Measurements were taken with a Tecan Genios Plus fluorescence plate reader in 10-min intervals for the first 30 min and then in 30-min intervals for 360 min.

NOX4-targeted cellular knockdown

Cells were incubated with 100 pfu/cell of Ad-siNOX4 in serum-free DMEM and then incubated with 5% fetal calf serum-supplemented DMEM for 24 h. After the initial incubation cells were transfected under the same conditions a second time. The knockdown efficiency of NOX4 was verified by qRT-PCR analysis. The primers used in the qRT-PCR determination were designed using the Beacon Designer software and synthesized at Integrated DNA Technologies (Coralville, IA, USA). The primer sequences used for NOX4 are as follows: forward primer—5′-CCTCTGATGTAATGGAACT-3′, reverse primer—5′-GGCAATGGAGAATAATATACTG-3′. RNA was isolated and the quantity determined using a Nanodrop 1000 spectrophotometer (ThermoFisher Scientific, Waltham, MA, USA). The primer specificity was determined by dissociation curve analysis after the polymerase reaction. GAPDH was used as the internal control, and the primer sequences for GAPDH were as follows: forward primer—5′-GCCTTCCGTGTTCCTACC-3′, reverse primer—5′-CTTCACCACCTTCTTGATGTC-3′.

Statistical analysis

All data are expressed as the mean ± SEM. Statistical analysis was performed using one-way ANOVA followed by Newman–Keuls multiple comparison test using the GraphPad Prism software package. Unpaired Student *t* test was used to determine statistical significance between two treatment groups. All experiments were repeated at least twice unless otherwise noted.

Results

ICAM-1 cytoplasmic tail increases endothelial cell intracellular GSH levels

Previous experiments in our lab using ICAM-1 gene-targeted mutant endothelial cells revealed increased GSH production [24]. The extracellular portion of ICAM-1 has been reported to undergo proteolytic cleavage in endothelial cells from these mice [29], suggesting that rather than a loss of extracellular ICAM-1 per se, the presence of the

intracellular cytoplasmic domain of ICAM-1 is important in regulating GSH. To test this hypothesis, two peptides were synthesized for the experiments performed in this study, the antennapedia internalization sequence (AP) [30] and the AP sequence coupled with the cytoplasmic tail (murine sequence, amino acids 500–535 [31]) of ICAM-1 (AP-ICAM) (Fig. 1A). Cells were treated for 6 h with increasing concentrations of AP-ICAM, and 25 μM was determined to be the optimal concentration for eliciting the maximal increase in intracellular GSH levels (Fig. 1B). A time course study of intracellular GSH levels in response to 25 μM AP-ICAM showed peak GSH levels at 6 h, which were decreased but still significant by 16 h (Fig. 1C). Moreover, addition of BSO, the specific inhibitor of GCL, attenuated GSH production in response to AP-ICAM (Fig. 1D).

ICAM-1 cytoplasmic tail increases endothelial GCL activity but not expression

Previous studies have shown that the amount of GCL enzyme present in the cell is correlated with de novo synthesis of GSH after stimulus by an oxidant [32,33]. Our previous studies using ICAM-1-deficient endothelial cells showed that increased GSH production correlates with increased Gclc expression and activity but those of not Gclm (modifier subunit of GCL) [24]. Thus, we measured the ability of AP-ICAM to alter GCL enzyme activity using the same temporal experimental design as for Fig. 1C and observed a significant increase in GCL activity over time, peaking at 8 h (Fig. 2A). Importantly, increased GCL activity at 6 h was attenuated by the addition of BSO (Fig. 2B). Increased GCL activity at 6 h did not correlate with an increase in Gclc protein expression, as shown by Western blot (Figs. 2C and D). These data suggest that AP-ICAM is able to increase GCL enzyme activity independent of altering enzyme protein levels.

Discrete proximal and distal regions of the ICAM-1 cytoplasmic tail regulate GSH production

In an effort to determine which AP-ICAM amino acid sequence motifs are responsible for increasing GSH levels, three variations of the AP-ICAM peptide were synthesized. As seen in Fig. 3A, TD1 comprises the AP, transmembrane, and PIP2/actinin/ezrin binding domain portions of the AP-ICAM peptide. TD2 comprises the AP, transmembrane, and terminal tail sequence of the AP-ICAM peptide. TD3 is made of the AP, the transmembrane, and an intermediate spanning sequence between the PIP2/actinin/ezrin and the terminal tail domains. Figs. 3B and C demonstrate a significant increase in GSH production as well as GCL activity when testing the TD1 and TD2 peptides but not the TD3 peptide. These data demonstrate that two discrete regions within the PIP2/actinin/ezrin domain and the terminal portion of the ICAM-1 cytoplasmic tail are involved in modulating endothelial cell GSH production.

ICAM-1 cytoplasmic tail increases endothelial ROS production

Cells treated with AP or AP-ICAM peptides were used in a DCF/ROS generation assay to determine if increased ROS were involved in altering intracellular GSH levels. Fig. 4A illustrates that AP-ICAM quickly increased DCF fluorescence, reaching a plateau at 30 min. The increase in ROS over time was attenuated by both apocynin, an ROS and NADPH oxidase inhibitor [34], and DPI, a flavoenzyme and NADPH oxidase inhibitor (Fig. 4B). We

next measured AP-ICAM-mediated $O_2^{\bullet -}$ production using hydroethidine treatment of cells in conjunction with peptide treatments over various time periods. Interestingly, AP-ICAM peptide treatment resulted in a significant biphasic early (30 min) and late (6 h) increase in $O_2^{\bullet -}$ production (2-OH-E adduct; Fig. 4C). Importantly, control AP peptide experiments resulted in a minor increase in superoxide production at 30 min but did not show an increase in superoxide production at 6 h. Importantly, Table 1 shows that despite the significant increases in superoxide production at 30 min and 6 h there was no significant change in the oxidation status of the proteins in the cell as measured by protein carbonyl formation. Treatment with PEG–catalase or PEG–SOD significantly abrogated AP-ICAM induction of DCF fluorescence levels (Fig. 4D). These data suggest that AP-ICAM initiates the formation of ROS, in the form of $O_2^{\bullet -}$, which can dismutate to hydrogen peroxide.

ICAM-1 cytoplasmic tail controls GSH/GCL fate through increased ROS levels

To determine if increased ROS production governs AP-ICAM induction of GSH production we examined the effect of apocynin or DPI on GSH levels and GCL activity. Fig. 5A shows that apocynin treatment blocked AP-ICAM-dependent increases in intracellular GSH. Similarly, apocynin inhibited AP-ICAM-mediated activation of GCL (Fig. 5B). Likewise, when DPI treatment was used, AP-ICAM was unable to induce an increase in GSH levels (Fig. 5C) or GCL activity (Fig. 5D). Together these data suggest that NADPH oxidase activity may serve an important role in the AP-ICAM induction of intracellular GSH levels and GCL activity.

ICAM-1 cytoplasmic tail affects GSH/GCL in a NADPH oxidase-dependent manner

Experiments performed thus far clearly identify the cytoplasmic tail of ICAM-1 as causing increased ROS levels (potentially through NADPH oxidase activity) leading to increased levels of GSH and GCL activity. Two NADPH oxidase isoforms (NOX2 and NOX4) are identified as being primarily located in endothelial cells [35], with NOX4 being highly expressed [36]. Quantitative real-time PCR analysis of NOX isoform expression in these endothelial cells revealed abundant NOX4 expression (data not shown). Therefore, we chose to target NOX4 for siRNA knockdown and were able to achieve a 70% decrease in mRNA expression (Fig. 6A). Knocking down NOX4 significantly attenuated the ability of AP-ICAM to produce GSH (Fig. 6B) and also significantly reduced GCL activity (Fig. 6C). These data clearly indicate NOX4 as playing a key role in increasing GSH levels and GCL activity after AP-ICAM treatment.

ICAM-1 cytoplasmic tail alters endothelial redox status via a PI3-kinase (PI3K) pathway

Langston et al. have recently shown that GSH production can be modulated through a PI3K-dependent pathway in response to insulin signaling [37]. Moreover, increased generation of intracellular ROS formation is known to alter PI3K activity [38,39]. Therefore, we examined whether the AP-ICAM-mediated alteration in GSH levels involved an ROS/PI3K pathway. Using two inhibitors of PI3K, wortmannin and LY 294002, we found that inhibition of PI3K significantly reduced GSH levels as well as GCL activity in AP-ICAM-treated endothelial cells (Figs. 7A and B, respectively). Surprisingly, inhibition of PI3K activity significantly decreased AP-ICAM induction of ROS production (Fig. 7C), indicating the PI3K activity is

responsible for ROS generation leading to elevated levels of GCL activity and therefore GSH levels, altering our paradigm to a PI3K/ROS-dependent pathway propagating the effect AP-ICAM has on the cell. We next determined the temporal nature of AP-ICAM induction of PI3K activity. AP-ICAM peptide treatment stimulated a small yet significant 20–30% increase in PI3K activity at 10 and 30 min, which was completely blunted by antioxidant treatment. Interestingly, PI3K activity was maximal (>2.3-fold increase) at 6 h, which was marginally affected by antioxidant treatment.

ICAM-1 cytoplasmic tail mediates VEGF-A-dependent endothelial cell migration

Last, we confirmed that the AP-ICAM peptide was biologically active in a GSH-sensitive in vitro angiogenesis model, as we have previously reported [22,24]. Treatment of cells with AP-ICAM significantly inhibited VEGF-A chemotaxis in a transwell cell migration assay, which was completely restored with BSO (Figs. 8A and B). These data are similar to those of our past studies using ICAM-1-deficient endothelial cells [22] and suggest a role for the cytoplasmic tail of ICAM-1 in regulating endothelial cell motility through a GSH-dependent pathway.

Discussion

In this study we have elucidated a novel endogenous oxidant/antioxidant inflammation-associated signaling mechanism by which the cytoplasmic tail of ICAM-1, using the AP-ICAM peptide, enhances GSH production within endothelial cells. AP-ICAM initiates ROS (superoxide and peroxide) production, activating PI3K, through a NOX4-dependent pathway, which in turn elevates GCL enzyme activity and GSH synthesis. Our results are unique and are the first to reveal an adhesion molecule-associated feedback mechanism that serves to regulate redox-dependent endothelial cell activation. The temporal peaks observed for maximal superoxide production and DCF signal (early—within 30–60 min) versus maximal PI3K activity (late—6 h) indicate that AP-ICAM mediates ROS→PI3K activation. Interestingly, we also observed a secondary late-phase increase in superoxide production at 6 h, which was coincident with increased PI3K activity at 6 h. Antioxidant treatment was unable to significantly block PI3K activity at the late time point, suggesting that PI3K activation could potentiate later ROS formation. Additional studies are needed to better understand this possible redox cycling process and to what extent it contributes to regulating endothelial cell redox status.

Identifying the cytoplasmic tail of ICAM-1 as the protein domain responsible for increased levels of GSH further clarifies lingering questions from our earlier studies. We previously reported similar cellular GSH responses when ICAM-1 on the surface of endothelial cells was ligated (by antibody or soluble ICAM-1 extracellular region) or deleted via gene-targeted mutation [22,23]. Together, these previous studies and our current findings reinforce the notion that the cytoplasmic tail of ICAM-1 plays a primary and important role in propagating signal responses involved in antioxidant defense, which regulates intracellular redox status.

The mechanistic basis of ICAM-1 cytoplasmic tail induction of GSH production seems to center on GCL activity, yet we did not observe significant differences in Gclc protein

expression, which is different from our findings with ICAM-1-deficient murine cells. This could be due to the fact that genetic manipulation results in a more long-lasting, permanent alteration of signal responses, which may influence Gclc expression independent of those identified here. Moreover, our current finding of increased GSH/GCL activity without increasing enzyme subunit expression could be due to an initial depletion of GSH in conjugation reactions leading to a loss of feedback inhibition of GCL present in the cell, something observed by others when treating cells with 4-hydroxynonenal [32]. It is also possible that increased GCL heterodimerization could explain the increase in de novo synthesis of GSH without altering subunit protein expression levels. Such an event would suggest that the AP-ICAM peptide elicits a PI3K/ROS signal allowing production of new GSH at levels below the threshold necessary for GCL subunit transcription. Future experiments are needed to better understand how AP-ICAM-1 peptide activates NOX4 activity in a PI3K-dependent manner.

Data demonstrating ICAM-1 cytoplasmic tail regulation of NOX4 activity and subsequent PI3K activity by cellular treatment with AP-ICAM peptide are novel. Previous studies have demonstrated that ROS formation enhances PI3K activity, yet terminal upstream initiators have remained largely unknown [38,39]. Until now, the key molecular targets and signaling pathways involved in modulating endothelial cell redox by inflammation-associated molecules remained incomplete. Our findings are the first to demonstrate endothelial cell redox regulation (ICAM-1 cytoplasmic tail > NOX4 > ROS > PI3K > GSH increase) in a temporal and progressive manner highlighting a novel endogenous antioxidant defense pathway that could be exploited biochemically to regulate endothelial cell redox status (Fig. 9). Last, it is not clear how AP-ICAM stimulates NOX4 activity. Several different molecular mediators could be involved in this response such as differential association with cytoskeleton linker molecules (e.g., α-actinin and ezrin) and increased intracellular calcium, all of which require further study [40].

Our observation that NOX4 leads to production of superoxide is unique as well; depending on model systems and method of analysis NOX4 has been observed to predominantly produce hydrogen peroxide [41,42]. However, previous studies have shown that endogenous siRNA knockdown of NOX4 significantly attenuates superoxide production [43,44]. Moreover, Ahmad et al. found that NOX4 plays an important role in contractile responses of bovine pulmonary arteries to hypoxia via superoxide-derived peroxide production [45]. These discrepancies could be due to the spatial location of NOX4 in relation to SOD allowing for rapid dismutation to peroxide as suggested by von Lohneysen et al. [41]. Another possibility is differences in detection techniques; in this study we used HPLC measurement that enables sensitive detection of small changes in superoxide levels, which was not employed in previous studies. Nonetheless, differences in basal versus activated cellular states, intracellular localization effects, and detection methods all require further investigation to determine specific responses of NOX4 activation.

Data showing that wortmannin and LY 294002 attenuate increases in intracellular levels of GSH are consistent with previous studies from other groups [46,47]. Langston et al. provided evidence of GSH modulation through a PI3K-dependent pathway in response to insulin signaling [37], and work from Mahadev et al. has demonstrated NOX4 as being

essential to insulin signal propagation [48]. The fact that these PI3K inhibitors also attenuate ROS production after AP-ICAM treatment shows that PI3K is a driving force responsible for induction of ROS leading to GSH synthesis. This observation is further confirmed by the fact that both apocynin (ROS and NADPH oxidase inhibitor) and DPI (NADPH oxidase inhibitor) are able to attenuate this increase in GSH. Previous data from our lab demonstrate a role for ICAM-1 in regulating PTEN expression and inhibiting cellular motility [22]. A study by Hamai et al. has recently reported that ICAM-1 expression modulates melanoma sensitivity to T cell cytotoxicity through decreasing PTEN activity, which increases Akt activity after increases in ICAM-1 expression [49]. Together, these observations suggest that ICAM-1 may elicit signaling responses in a redox-dependent manner that may differentially alter PTEN activation thereby influencing cellular motility and survival in a GSH-dependent manner. Additional studies will be needed to clearly address how PI3K activity is regulated in response to AP-ICAM treatment and what, if any, role PTEN function plays in this response.

In summary, our findings show that ICAM-1, through NOX4 activation, increases ROS production and PI3K activity resulting in increased GCL activity and GSH synthesis. Our data are biologically relevant to several disease states involving angiogenesis and inflammation as AP-ICAM induction of GSH synthesis was able to inhibit VEGF-A-dependent endothelial cell chemotaxis, suggesting these molecules may be therapeutically useful. Understanding the redox relationship between endogenous antioxidant defense pathways and endothelial cell activation is essential if we are to harness redox biology for the development of novel cardiovascular disease therapies.

Acknowledgments

This work was supported by NIH Grants HL080482 to C.G.K and HL094021 to C.B.P. C.G.K., C.B.P., and S.P. have filed a provisional patent regarding AP-ICAM peptide function and composition.

References

1. Ushio-Fukai M. Redox signaling in angiogenesis: role of NADPH oxidase. Cardiovasc. Res. 2006; 71:226–235. [PubMed: 16781692]
2. Doyle B, Caplice N. Plaque neovascularization and antiangiogenic therapy for atherosclerosis. J. Am. Coll. Cardiol. 2007; 49:2073–2080. [PubMed: 17531655]
3. Miura S, Fujino M, Matsuo Y, Kawamura A, Tanigawa H, Nishikawa H, Saku K. High density lipoprotein-induced angiogenesis requires the activation of Ras/MAP kinase in human coronary artery endothelial cells. Arterioscler. Thromb. Vasc. Biol. 2003; 23:802–808. [PubMed: 12637339]
4. Carmeliet P. Angiogenesis in health and disease. Nat. Med. 2003; 9:653–660. [PubMed: 12778163]
5. Adachi T, Cohen RA. Decreased aortic glutathione levels may contribute to impaired nitric oxide-induced relaxation in hypercholesterolaemia. Br. J. Pharmacol. 2000; 129:1014–1020. [PubMed: 10696103]
6. Griffith OW. Biologic and pharmacologic regulation of mammalian glutathione synthesis. Free Radic. Biol. Med. 1999; 27:922–935. [PubMed: 10569625]
7. Dulak J, Loboda A, Jozkowicz A. Effect of heme oxygenase-1 on vascular function and disease. Curr. Opin. Lipidol. 2008; 19:505–512. [PubMed: 18769232]
8. Ballatori N, Krance SM, Notenboom S, Shi S, Tieu K, Hammond CL. Glutathione dysregulation and the etiology and progression of human diseases. Biol. Chem. 2009; 390:191–214. [PubMed: 19166318]

9. Brandes RP, Schroder K. Differential vascular functions of Nox family NADPH oxidases. Curr. Opin. Lipidol. 2008; 19:513–518. [PubMed: 18769233]
10. Vartanian SM, Sarkar R. Therapeutic angiogenesis. Vasc. Endovasc. Surg. 2007; 41:173–185.
11. Chua CC, Hamdy RC, Chua BH. Upregulation of vascular endothelial growth factor by H2O2 in rat heart endothelial cells. Free Radic. Biol. Med. 1998; 25:891–897. [PubMed: 9840733]
12. Chen JX, Zeng H, Tuo QH, Yu H, Meyrick B, Aschner JL. NADPH oxidase modulates myocardial Akt, ERK1/2 activation, and angiogenesis after hypoxia–reoxygenation. Am. J. Physiol. 2007; 292:H1664–H1674.
13. Matsumoto T, Claesson-Welsh L. VEGF receptor signal transduction. Sci. STKERE21. 2001
14. Ushio-Fukai M. VEGF signaling through NADPH oxidase-derived ROS. Antioxid. Redox Signaling. 2007; 9:731–739.
15. Maulik N, Das DK. Redox signaling in vascular angiogenesis. Free Radic. Biol. Med. 2002; 33:1047–1060. [PubMed: 12374616]
16. Ojha N, Roy S, He G, Biswas S, Velayutham M, Khanna S, Kuppusamy P, Zweier JL, Sen CK. Assessment of wound-site redox environment and the significance of Rac2 in cutaneous healing. Free Radic. Biol. Med. 2007; 44:682–691. [PubMed: 18068132]
17. Tojo T, Ushio-Fukai M, Yamaoka-Tojo M, Ikeda S, Patrushev N, Alexander RW. Role of gp91phox (Nox2)-containing NAD(P)H oxidase in angiogenesis in response to hindlimb ischemia. Circulation. 2005; 111:2347–2355. [PubMed: 15867174]
18. Roy S, Khanna S, Nallu K, Hunt TK, Sen CK. Dermal wound healing is subject to redox control. Mol. Ther. 2006; 13:211–220. [PubMed: 16126008]
19. Radisavljevic Z, Avraham H, Avraham S. Vascular endothelial growth factor up-regulates ICAM-1 expression via the phosphatidylinositol 3 OH-kinase/AKT/nitric oxide pathway and modulates migration of brain microvascular endothelial cells. J. Biol. Chem. 2000; 275:20770–20774. [PubMed: 10787417]
20. DeLisser HM, Christofidou-Solomidou M, Strieter RM, Burdick MD, Robinson CS, Wexler RS, Kerr JS, Garlanda C, Merwin JR, Madri JA, Albelda SM. Involvement of endothelial PECAM-1/CD31 in angiogenesis. Am. J. Pathol. 1997; 151:671–677. [PubMed: 9284815]
21. Huang MT, Mason JC, Birdsey GM, Amsellem V, Gerwin N, Haskard DO, Ridley AJ, Randi AM. Endothelial intercellular adhesion molecule (ICAM)-2 regulates angiogenesis. Blood. 2005; 106:1636–1643. [PubMed: 15920013]
22. Langston W, Chidlow JH Jr, Booth BA, Barlow SC, Lefer DJ, Patel RP, Kevil CG. Regulation of endothelial glutathione by ICAM-1 governs VEGF-A-mediated eNOS activity and angiogenesis. Free Radic. Biol. Med. 2007; 42:720–729. [PubMed: 17291995]
23. Pruitt HM, Langston W, Kevil CG, Patel RP. ICAM-1 cross-linking stimulates endothelial glutathione synthesis. Antioxid. Redox Signaling. 2007; 9:159–164.
24. Kevil CG, Orr AW, Langston W, Mickett K, Murphy-Ullrich J, Patel RP, Kucik DF, Bullard DC. Intercellular adhesion molecule-1 (ICAM-1) regulates endothelial cell motility through a nitric oxide-dependent pathway. J. Biol. Chem. 2004; 279:19230–19238. [PubMed: 14985356]
25. King PD, Sandberg ET, Selvakumar A, Fang P, Beaud AL, Dupont B. Novel isoforms of murine intercellular adhesion molecule-1 generated by alternative RNA splicing. J. Immunol. 1995; 154:6080–6093. [PubMed: 7751650]
26. Tsakadze NL, Zhao Z, D'Souza SE. Interactions of intercellular adhesion molecule-1 with fibrinogen. Trends Cardiovasc. Med. 2002; 12:101–108. [PubMed: 12007734]
27. White CC, Viernes H, Krejsa CM, Botta D, Kavanagh TJ. Fluorescence-based microtiter plate assay for glutamate–cysteine ligase activity. Anal. Biochem. 2003; 318:175–180. [PubMed: 12814619]
28. Zielonka J, Vasquez-Vivar J, Kalyanaraman B. Detection of 2-hydroxyethidium in cellular systems: a unique marker product of superoxide and hydroethidine. Nat. Protoc. 2008; 3:8–21. [PubMed: 18193017]
29. van Den Engel NK, Heidenthal E, Vinke A, Kolb H, Martin S. Circulating forms of intercellular adhesion molecule (ICAM)-1 in mice lacking membranous ICAM-1. Blood. 2000; 95:1350–1355. [PubMed: 10666210]

30. Gallouzi IE, Steitz JA. Delineation of mRNA export pathways by the use of cell-permeable peptides. Science. 2001; 294:1895–1901. [PubMed: 11729309]
31. Manning AM, Lu HF, Kukielka GL, Oliver MG, Ty T, Toman CA, Drong RF, Slightom JL, Ballantyne CM, Entman ML, et al. Cloning and comparative sequence analysis of the gene encoding canine intercellular adhesion molecule-1 (ICAM-1). Gene. 1995; 156:291–295. [PubMed: 7758971]
32. Iles KE, Liu RM. Mechanisms of glutamate cysteine ligase (GCL) induction by 4-hydroxynonenal. Free Radic. Biol. Med. 2005; 38:547–556. [PubMed: 15683710]
33. Choi J, Liu RM, Forman HJ. Adaptation to oxidative stress: quinone-mediated protection of signaling in rat lung epithelial L2 cells. Biochem. Pharmacol. 1997; 53:987–993. [PubMed: 9174112]
34. Heumuller S, Wind S, Barbosa-Sicard E, Schmidt HH, Busse R, Schroder K, Brandes RP. Apocynin is not an inhibitor of vascular NADPH oxidases but an antioxidant. Hypertension. 2008; 51:211–217. [PubMed: 18086956]
35. Dworakowski R, Alom-Ruiz SP, Shah AM. NADPH oxidase-derived reactive oxygen species in the regulation of endothelial phenotype. Pharmacol. Rep. 2008; 60:21–28. [PubMed: 18276982]
36. Sorescu D, Weiss D, Lassegue B, Clempus RE, Szocs K, Sorescu GP, Valppu L, Quinn MT, Lambeth JD, Vega JD, Taylor WR, Griendling KK. Superoxide production and expression of Nox family proteins in human atherosclerosis. Circulation. 2002; 105:1429–1435. [PubMed: 11914250]
37. Langston W, Circu ML, Aw TY. Insulin stimulation of γ-glutamylcysteine ligase catalytic subunit expression increases endothelial GSH during oxidative stress: influence of low glucose. Free Radic. Biol. Med. 2008; 45:1591–1599. [PubMed: 18926903]
38. Zou CG, Gao SY, Zhao YS, Li SD, Cao XZ, Zhang Y, Zhang KQ. Homocysteine enhances cell proliferation in hepatic myofibroblastic stellate cells. J. Mol. Med. 2009; 87:75–84. [PubMed: 18825355]
39. Song S, Guha S, Liu K, Buttar NS, Bresalier RS. COX-2 induction by unconjugated bile acids involves reactive oxygen species-mediated signalling pathways in Barrett's oesophagus and oesophageal adenocarcinoma. Gut. 2007; 56:1512–1521. [PubMed: 17604323]
40. Rahman A, Fazal F. Hug tightly and say goodbye: role of endothelial ICAM-1 in leukocyte transmigration. Antioxid. Redox Signaling. 2009; 11:823–839.
41. von Lohneysen K, Noack D, Jesaitis AJ, Dinauer MC, Knaus UG. Mutational analysis reveals distinct features of the Nox4-p22 phox complex. J. Biol. Chem. 2008; 283:35273–35282. [PubMed: 18849343]
42. Dikalov SI, Dikalova AE, Bikineyeva AT, Schmidt HH, Harrison DG, Griendling KK. Distinct roles of Nox1 and Nox4 in basal and angiotensin II-stimulated superoxide and hydrogen peroxide production. Free Radic. Biol. Med. 2008; 45:1340–1351. [PubMed: 18760347]
43. Block K, Gorin Y, Abboud HE. Subcellular localization of Nox4 and regulation in diabetes. Proc. Natl. Acad. Sci. U. S. A. 2009; 106:14385–14390. [PubMed: 19706525]
44. Cucoranu I, Clempus R, Dikalova A, Phelan PJ, Ariyan S, Dikalov S, Sorescu D. NAD(P)H oxidase 4 mediates transforming growth factor-beta1-induced differentiation of cardiac fibroblasts into myofibroblasts. Circ. Res. 2005; 97:900–907. [PubMed: 16179589]
45. Ahmad M, Kelly MR, Zhao X, Kandhi S, Wolin MS. Roles for Nox4 in the contractile response of bovine pulmonary arteries to hypoxia. Am. J. Physiol. Heart Circ. Physiol. 2010; 298:H1879–H1888. [PubMed: 20304813]
46. Arisawa S, Ishida K, Kameyama N, Ueyama J, Hattori A, Tatsumi Y, Hayashi H, Yano M, Hayashi K, Katano Y, Goto H, Takagi K, Wakusawa S. Ursodeoxycholic acid induces glutathione synthesis through activation of PI3K/Akt pathway in HepG2 cells. Biochem. Pharmacol. 2008; 77:858–866. [PubMed: 19073151]
47. Kim SK, Woodcroft KJ, Khodadadeh SS, Novak RF. Insulin signaling regulates gamma-glutamylcysteine ligase catalytic subunit expression in primary cultured rat hepatocytes. J. Pharmacol. Exp. Ther. 2004; 311:99–108. [PubMed: 15169830]
48. Mahadev K, Motoshima H, Wu X, Ruddy JM, Arnold RS, Cheng G, Lambeth JD, Goldstein BJ. The NAD(P)H oxidase homolog Nox4 modulates insulin-stimulated generation of H2O2 and plays

an integral role in insulin signal transduction. Mol. Cell. Biol. 2004; 24:1844–1854. [PubMed: 14966267]

49. Hamai A, Meslin F, Benlalam H, Jalil A, Mehrpour M, Faure F, Lecluse Y, Vielh P, Avril MF, Robert C, Chouaib S. ICAM-1 has a critical role in the regulation of metastatic melanoma tumor susceptibility to CTL lysis by interfering with PI3K/AKT pathway. Cancer Res. 2008; 68:9854–9864. [PubMed: 19047166]

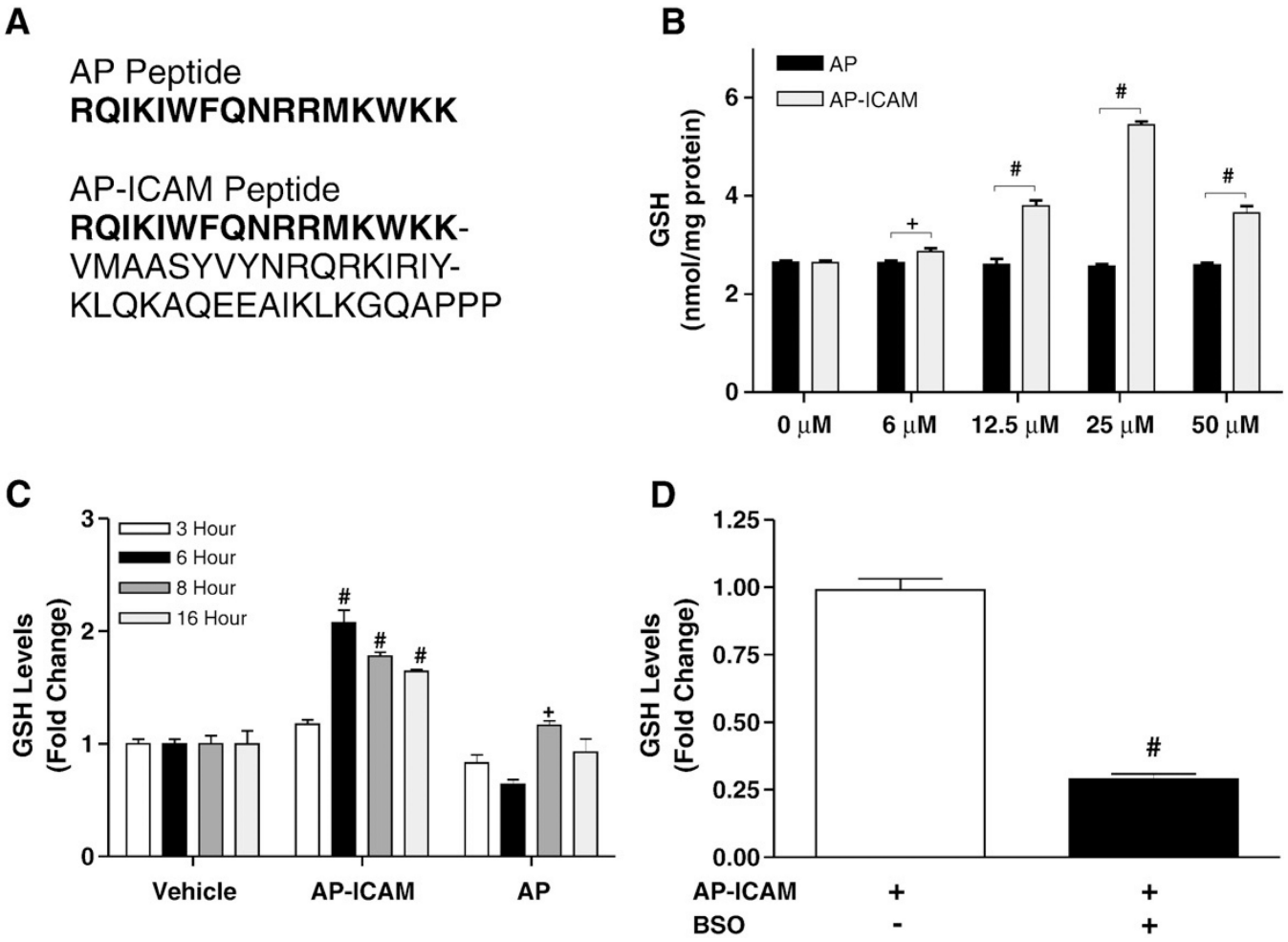

Fig. 1.

The cytoplasmic tail of ICAM-1 increases production of GSH in a time-dependent manner. (A) The amino acid sequences of the AP and AP-ICAM peptides. (B) GSH levels after cellular treatment with various concentrations of the cytoplasmic tail peptide AP-ICAM. (C) GSH levels measured at various time points after cellular treatment with AP or AP-ICAM peptide (normalized to vehicle). (D) GSH levels after treatment with the AP-ICAM peptide plus BSO (normalized to AP-ICAM treatment alone). n=5; #p<0.001, + p<0.05; experiments performed in quadruplicate.

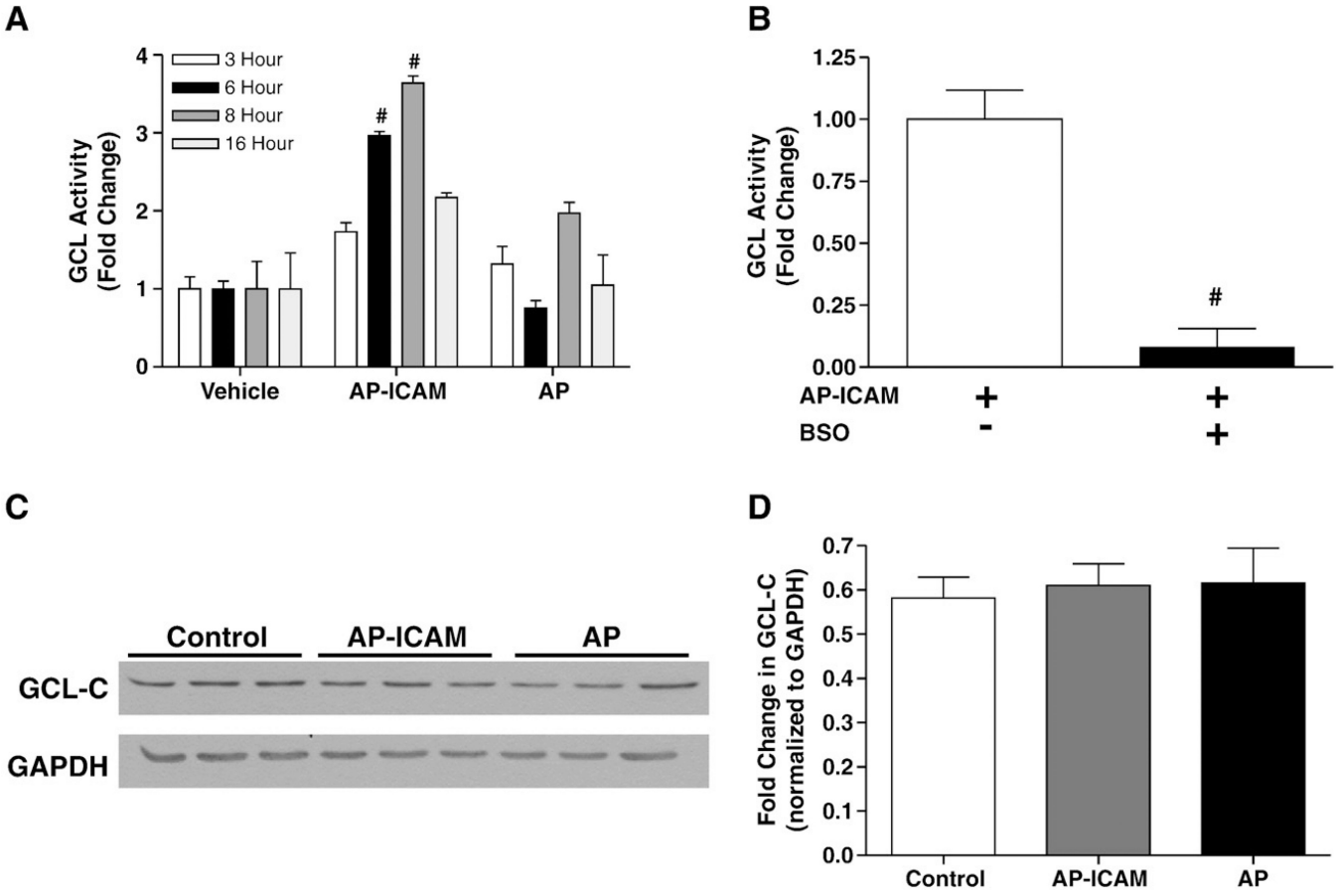

Fig. 2.

The cytoplasmic tail of ICAM-1 increases GCL activity, but not enzyme subunit protein expression. (A) GCL activity measured at various time points after cellular treatment with AP or AP-ICAM peptide (normalized to vehicle). (B) GCL activity after cellular treatment with the AP-ICAM peptide plus BSO (normalized to AP-ICAM treatment alone). (C and D) Western blot and quantitation comparing levels of Gclc protein in cells at 6 h posttreatment with AP-ICAM or AP peptide. n=5, #p<0.001, experiments performed in quadruplicate, Western blots performed in triplicate.

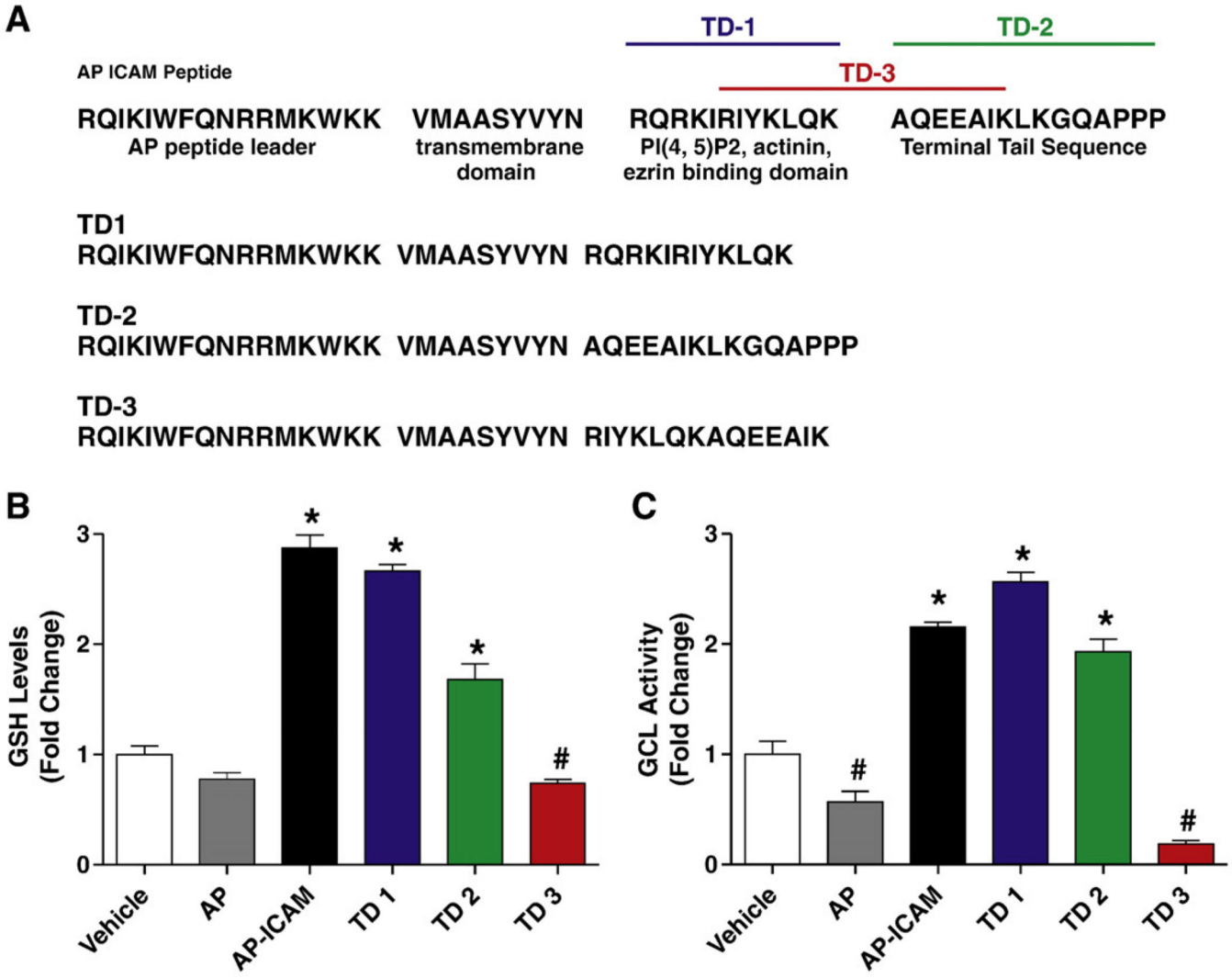

Fig. 3.

Various portions of the ICAM-1 cytoplasmic tail modulate both GSH levels and GCL activity. (A) The complete amino acid sequence for the AP-ICAM as well as TD1, TD2, and TD3 peptides in conjunction with the purported function of each segment. (B) GSH levels after cellular treatment with AP-ICAM and the three variations of the cytoplasmic tail peptide. (C) GCL activity after cellular treatment with AP-ICAM and the three variations of the cytoplasmic tail peptide. n=5; #p<0.001, *p<0.01; experiments performed in quadruplicate.

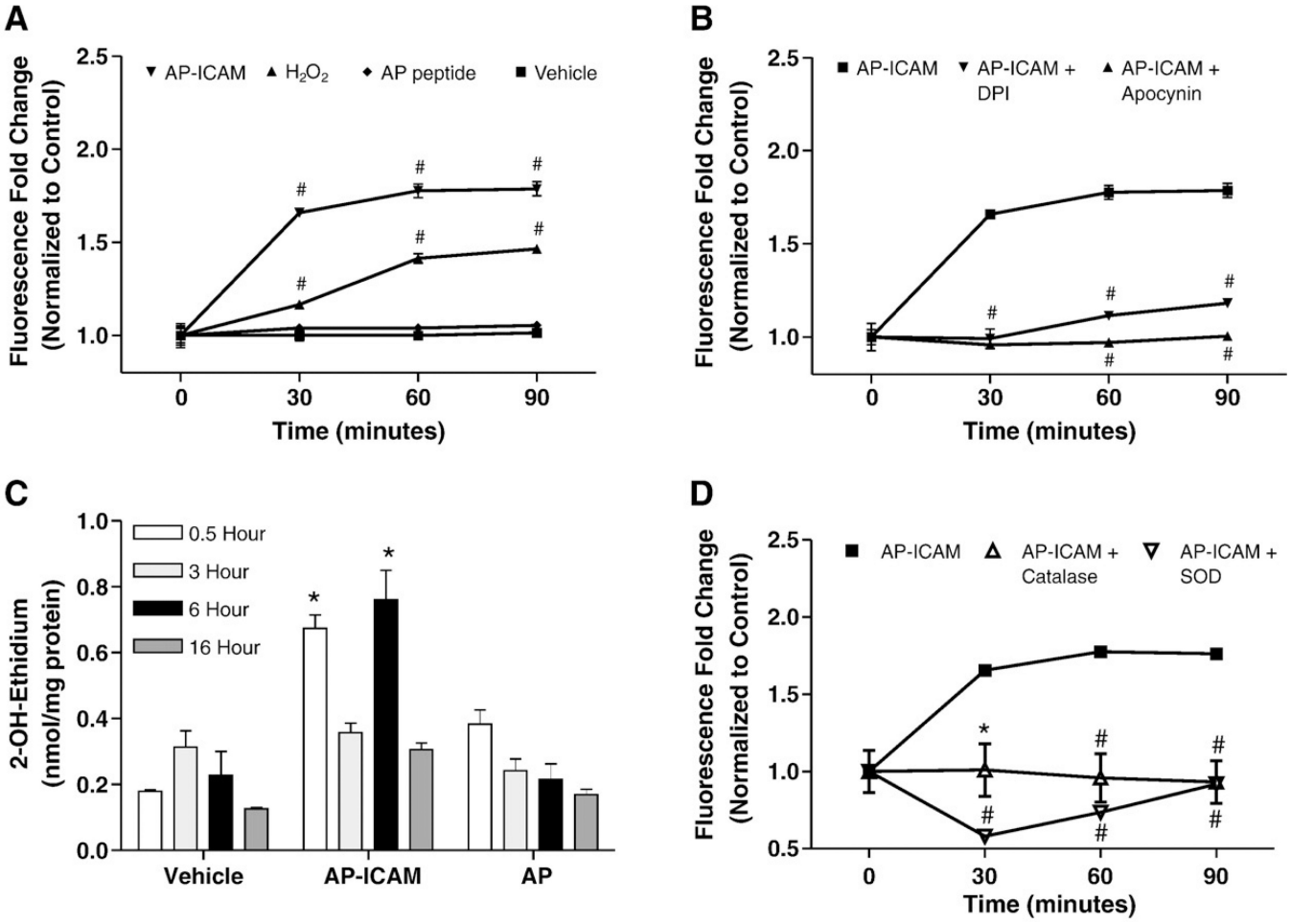

Fig. 4.

The cytoplasmic tail of ICAM-1 increases cellular ROS production. (A) DCF assay showing increased ROS production in response to AP-ICAM treatment over time compared to AP peptide, hydrogen peroxide (50 μM), and vehicle treatments. (B) Changes in DCF fluorescence between AP-ICAM-treated cells and AP-ICAM treatment plus DPI (1 μM) or apocynin (100 μM). (C) HPLC measurement of superoxide formation from 2-OH-ethidium levels after various peptide treatments at different time points, which were compared to respective time controls. (D) Changes in DCF fluorescence between AP-ICAM and AP-ICAM plus PEG–SOD (400 units/ml) or PEG–catalase (100 units/ml). n=4; #p<0.001, *p<0.01; DCF experiments performed in quadruplicate and 2-OH-ethidium experiments were performed in duplicate.

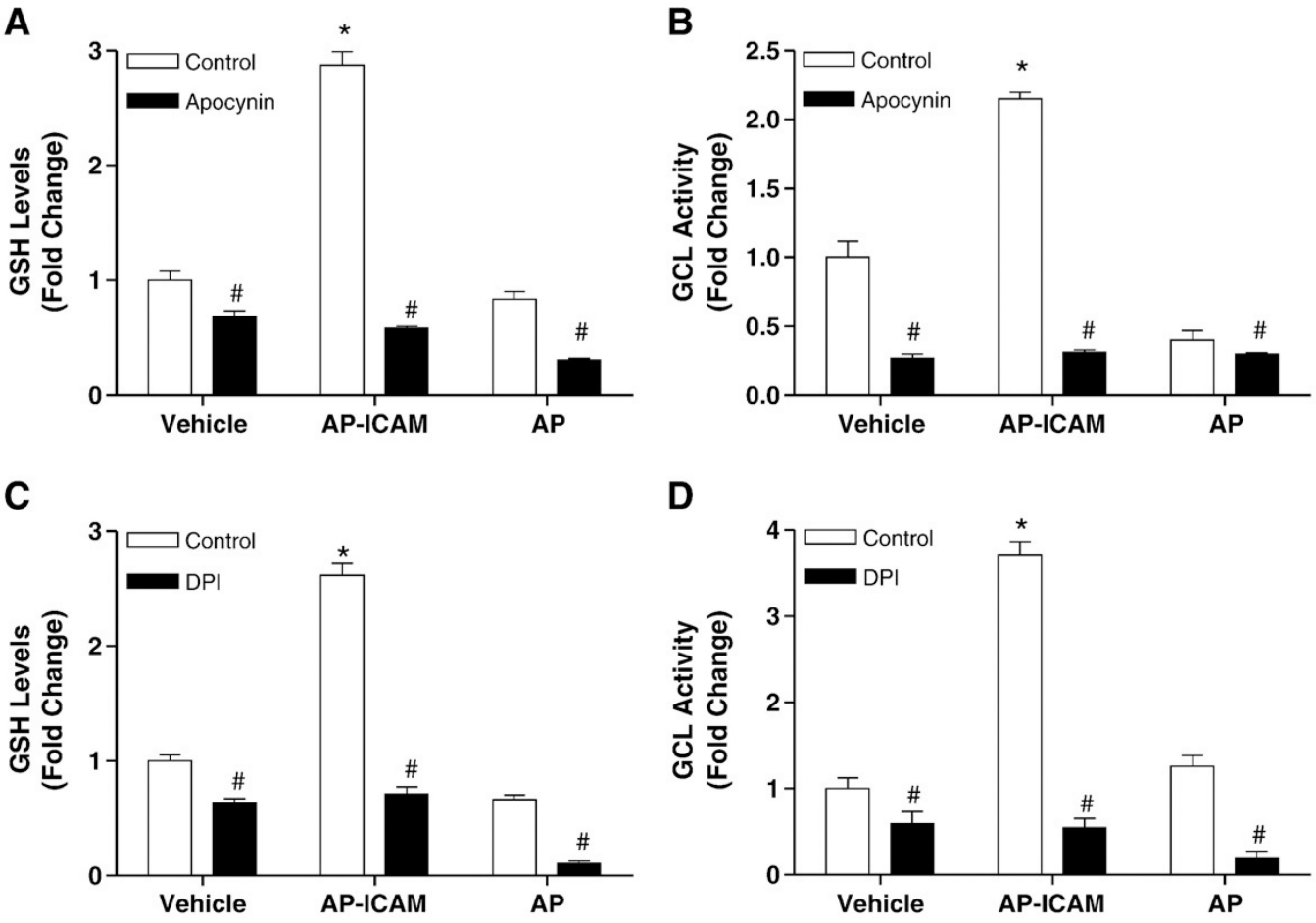

Fig. 5.

Treatment with apocynin, as well as DPI, attenuates intracellular GSH production and GCL activity by ICAM-1 cytoplasmic tail peptide. (A) GSH levels in response to AP-ICAM, AP, or vehicle plus apocynin (100 μM) versus the same treatments alone. (B) GCL activity in response to AP-ICAM, AP, or vehicle plus apocynin (100 μM) versus AP-ICAM treatment alone. (C) GSH levels in response to AP-ICAM, AP, or vehicle plus DPI (1 μM) versus the same treatments alone. (D) GCL activity in response to AP-ICAM, AP, or vehicle plus DPI (1 μM) versus the same treatments alone. n=5; #p<0.001, *p<0.01; experiments performed in quadruplicate.

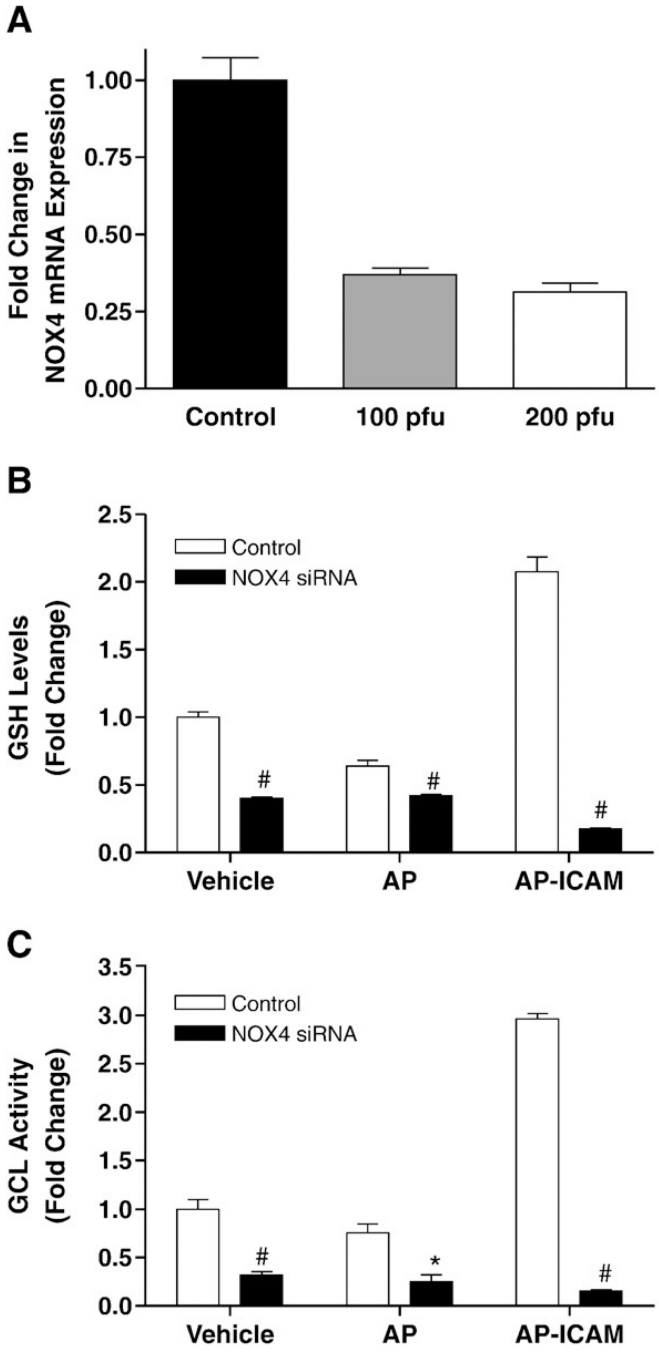

Fig. 6.

Decreasing NOX4 expression attenuates AP-ICAM induction of increased GSH and GCL activity. (A) The decrease in NOX4 mRNA expression after NOX4 siRNA administration is shown. (B) The effect of targeted NOX4 knockdown on GSH production in response to vehicle, AP, or AP-ICAM peptide treatment (normalized to vehicle). (C) The effect of targeted NOX4 knockdown on GCL activity in response to vehicle, AP, or AP-ICAM peptide treatment (normalized to vehicle). n=5; #p<0.001, *p<0.01; experiments performed in quadruplicate.

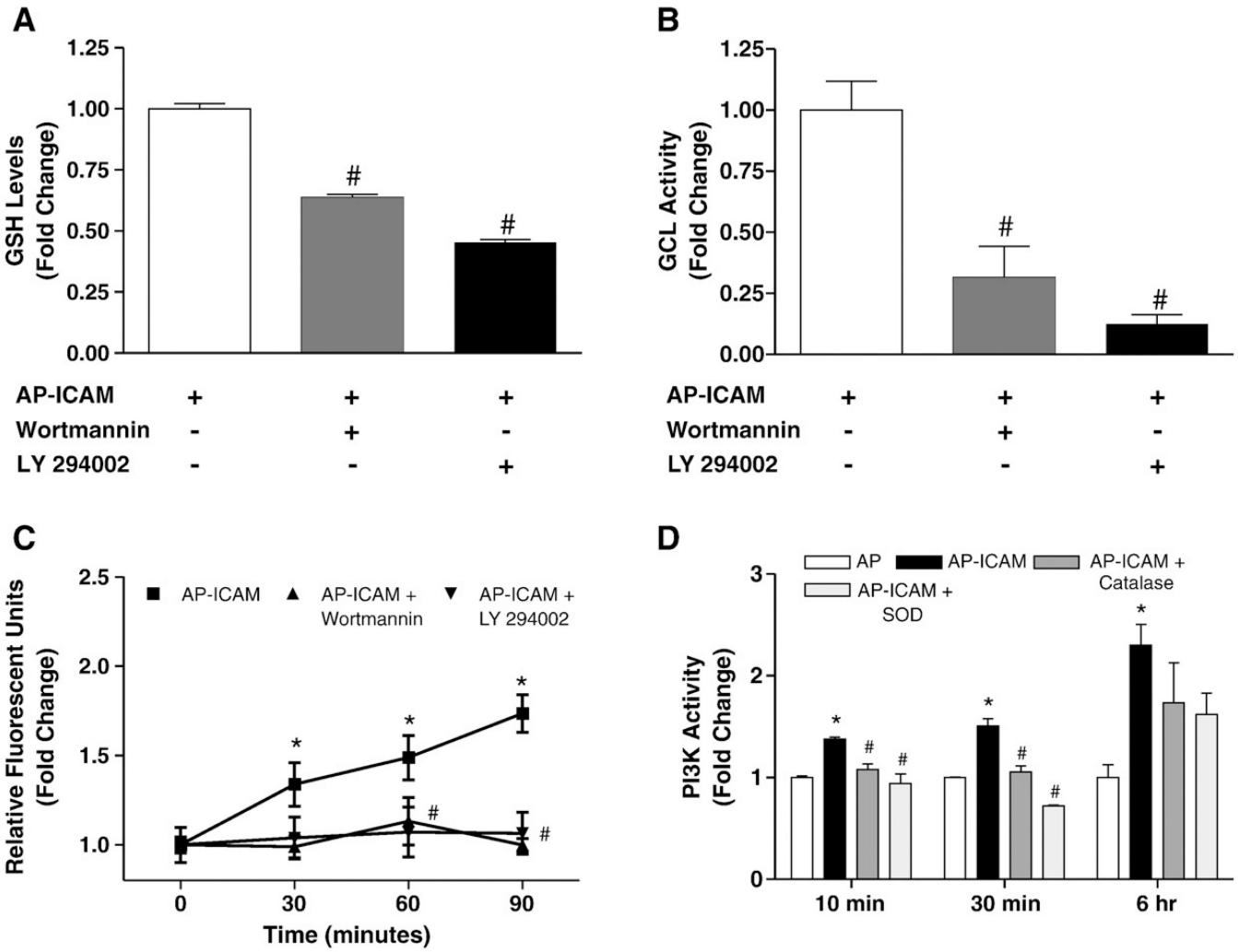

Fig. 7.

AP-ICAM peptide increases PI3 kinase activity, which modulates intracellular GSH production and GCL activity. (A) GSH levels after cellular treatment with AP-ICAM peptide plus either wortmannin (6 μM) or LY 294002 (20 μM) (normalized to AP-ICAM treatment alone). (B) GCL activity after cellular treatment with the AP-ICAM peptide plus wortmannin (6 μM) or LY 294002 (20 μM) (normalized to AP-ICAM treatment alone). (C) Changes in DCF fluorescence between AP-ICAM and AP-ICAM plus wortmannin (6 μM) or LY 294002 (20 μM). (D) Changes in PI3K activity after AP-ICAM treatment with or without PEG–SOD or PEG–catalase at various time points. n=5, #p<0.001 versus AP-ICAM alone, *p<0.01 versus AP peptide or time 0 min, experiments performed in triplicate.

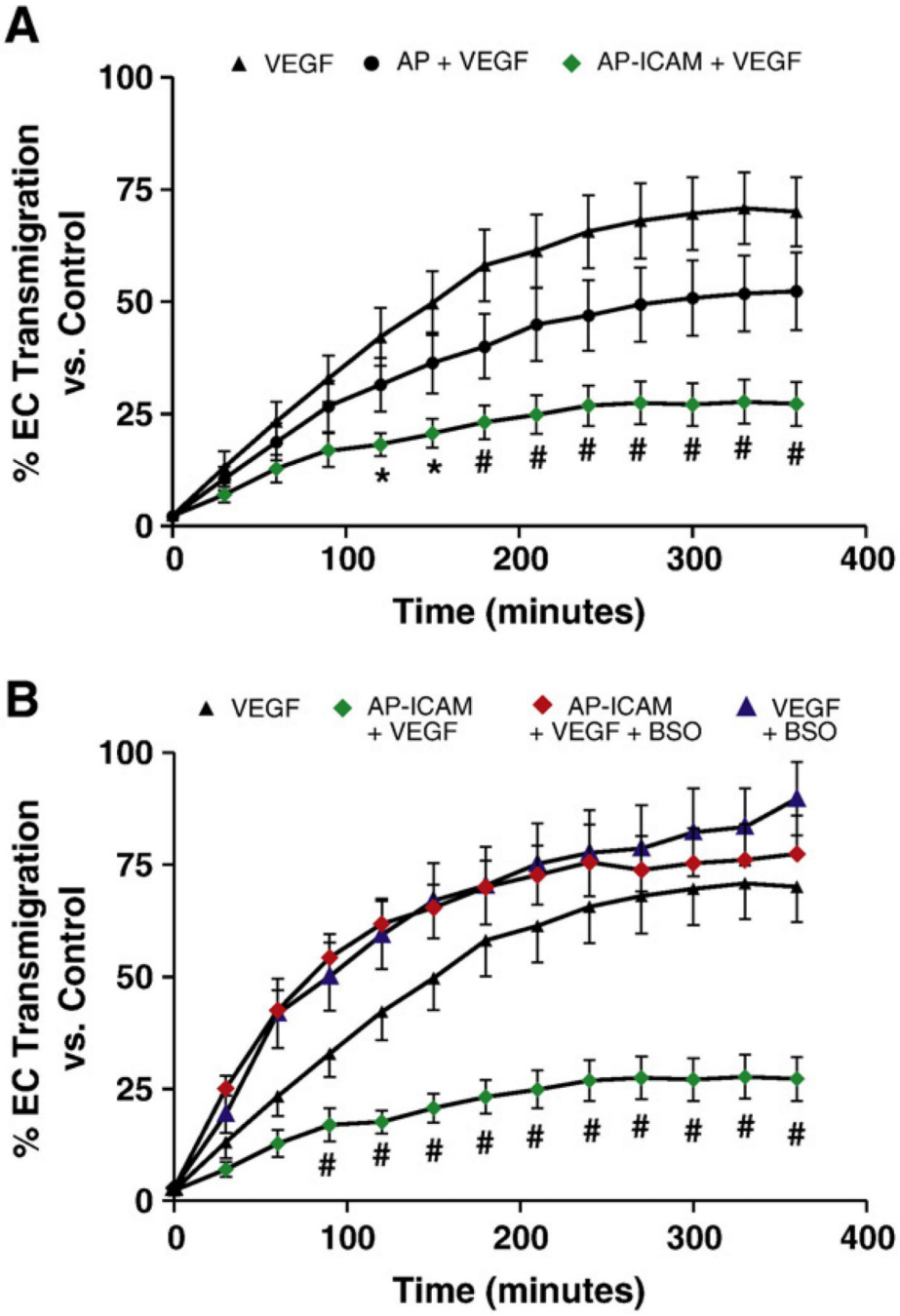

Fig. 8.

AP-ICAM peptide blocks VEGF-dependent chemotaxis in a glutathione-dependent manner. (A) The percentage of endothelial cell transmigration over time in response to VEGF-A (50 ng/ml), VEGF-A plus AP (25 μM) peptide, or VEGF-A plus AP-ICAM (25 μM) peptide. (B) The effect of BSO treatment (150 μM) on VEGF-A chemotaxis with or without peptide treatment. n=5; #p<0.001, *p<0.01; experiments performed in triplicate.

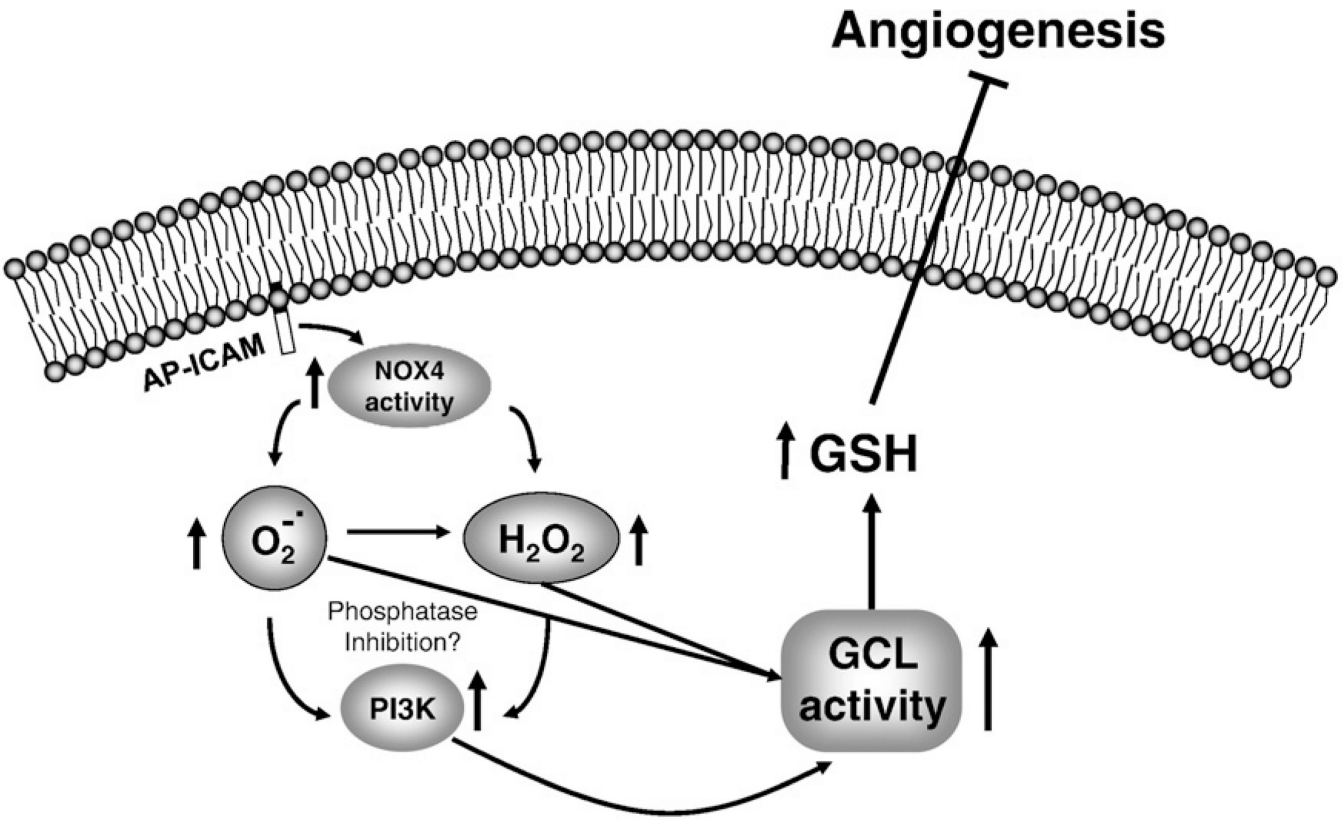

Fig. 9.
Proposed mechanism of endothelial cell redox regulation by ICAM-1.

Table 1

Temporal protein carbonyl levels in response to AP-ICAM peptide

	0.5 h	3 h	6 h
Control (nmol/mg)	3.84±0.14	3.84±0.12	3.40±0.76
AP-ICAM (nmol/mg)	3.50±0.27	4.02±0.23	3.79±0.12
AP (nmol/mg)	3.64±0.41	3.96±0.23	3.75±0.29

Protein carbonyl formation 30 min, 3 h, and 6 h after addition of AP-ICAM to cell culture.